RSC Advances

PAPER

View Article Online
View Journal | View Issue

Cite this: *RSC Adv.*, 2017, **7**, 35004

Simple synthesis of ZnO nanoparticles on N-doped reduced graphene oxide for the electrocatalytic sensing of L-cysteine

Suling Yang, *[ab] Gang Li,[a] Chen Qu,[c] Guifang Wang[a] and Dan Wang[a]

Received 10th April 2017
Accepted 25th June 2017

DOI: 10.1039/c7ra04052k

rsc.li/rsc-advances

A new kind of ZnO nanoparticle/N-doped reduced graphene oxide nanocomposite (ZnONPs/N-rGO) was synthesized through a low temperature, low-cost and one step hydrothermal process. By using the prepared nanocomposite as a modified electrode material, an L-cysteine electrochemical sensor was fabricated. X-ray diffraction, transmission electron microscopy, scanning electron microscopy, X-ray photoelectron spectroscopy and electrochemical techniques were used to study the nanocomposite. The nanocomposite shows a high electro-catalytic activity toward L-cysteine oxidation. Under the optimum determination conditions, the nanocomposite modified electrode provided L-cysteine with a broad detection range of 0.1–705.0 μM and a limit of detection of 0.1 μM (S/N = 3). This novel method was successfully used to determine L-cysteine in real samples.

1. Introduction

L-Cysteine is a semi-essential amino acid that plays a crucial biological role in numerous important cellular functions, including protein production, the metabolism of many essential bio-reagents (*e.g.* coenzyme A, biotin and lipoid acid), bio-redox performance and detoxification.[1] A deficiency of L-cysteine can result in a number of different syndromes, such as retarded growth in childhood, hair depigmentation, skin damage, liver harm, edema and myasthenia.[2] In addition, the abnormal formation and accumulation of cysteine are expressed by metabolic disorders, cystinosis, neurological pathogeneses, and Alzheimer's and Parkinson's diseases.[3] Therefore, the development of a method for detecting L-cysteine with high sensitivity and selectivity is necessary from a clinical point of view. At present, some techniques, such as HPLC,[4] fluorescent methods,[5] spectrophotometric methods[6] and chemiluminescence[7] have already been developed to detect L-cysteine in biological and pharmaceutical samples, but many of the mentioned methods are either complicated or lacking in selectivity. Compared with other methods, electrochemical method shows many advantages, such as simple operation, inexpensive consumption, good selectivity and convenient real-time determination. On the conventional electrode, L-cysteine displays either poor response or high overpotential owing to the formation of surface oxide, which would result in narrow detecting range and low selectivity. Currently, various modified electrodes with excellent electrocatalytic characteristics have been developed for the detection of L-cysteine, for example, carbon-based electrodes (*e.g.*, graphene[8] and carbon nanotube[9]), metal-based electrodes (*e.g.*, Au,[10] Ag–Pd[11] and Au[12]), metal oxide-based electrodes (*e.g.*, Cu_2O,[13] MnO_x (ref. 14) and RuO_2 (ref. 15)), and polymer-based electrodes (*e.g.*, polypyrrole,[8] poly-eriochrome black T[10] and poly(4-vinylpyridine)[16]) *et al.* However, the lower limit of detection, wider linear range and higher sensibility are expected to be realized. Therefore, it is necessary to develop novel materials to improve the electrochemical performance for the L-cysteine detection.

ZnO, as a semiconductor with wide band gap, has get more attention due to its suitable band gap (3.37 eV) at room temperature and high electron mobility (200–300 $cm^{-2}\,V^{-1}\,s^{-1}$), which promotes electron transfer efficiency.[17,18] ZnO has been widely used in electrochemical sensor because of its relatively open structure, high electron mobility and thermal stability. Xia *et al.*[19] reported the synthesis of ZnO flowers, and found that this material provided both high sensitivity and selectivity for the direct determination of dopamine in the presence of ascorbic acid. Khun *et al.*[20] synthesized ZnO/CuO nanocomposite, which grown on the gold-coated glass substrate, and they investigated the electrochemical detection of DA by using the prepared nanocomposite. These reports indicate that ZnO-based materials could offer opportunities for the selective and sensitive electrochemical application. However, semiconductor ZnO has poor electronic conductivity, which greatly limits the improvement in electrochemical application. Considering this fact, the combination of ZnO with graphene may be an ideal

[a]College of Chemistry and Chemical Engineering, Anyang Normal University, Anyang 455002, PR China. E-mail: yang_suling@163.com; Fax: +86 3722900040; Tel: +86 03722900040

[b]Henan Key Laboratory of Biomolecular Recognition and Sensing, Shangqiu Normal University, Shangqiu 476000, PR China

[c]Department of Chemical and Biomolecular Engineering, University of Notre Dame, 220 Main Building Notre Dame, IN 46556-5602, Indiana—IN, USA

strategy to exhibit superior electro-catalytic performance because graphene can facilitate the charge transfer in the electro-catalytic process. Jiang *et al.*[21] prepared ZnO nanocrystals on N-doped graphene for electrochemiluminescence detection of pentachlorophenol by using glycine as N source, under 500 °C argon atmosphere in an alumina crucible; but this method has some deficiencies, such as high temperature (500 °C) and harsh operating environments (argon protection). So, it is necessary to develop a technique for the synthesis of nanostructure ZnO decorated with N-doped graphene by using low temperature, low-cost and one step procedure.

Graphene, a single layer carbon atoms formed into a benzene-ring structure, has provided an ideal electrochemical platform for the fabrication of L-cysteine biosensors due to its specific surface area, high electron conductivity, good biocompatibility, stability and inexpensive production. The graphene-based L-cysteine biosensors have been constructed by numerous methods and employed for electrochemical detection of L-cysteine, which exhibited good selectivity and sensitivity compared to most conventional L-cysteine biosensors.[8,14] However, doping of graphene with hetero-atoms (*e.g.*, N, P, B, S *etc.*) can effectively modulate its electrochemical properties and increase its electro-catalytic performances.[22–24] It has been indicated that the electrochemical active sites introduced by doped hetero-atoms are advantageous for the adsorption and activation of analysts through the combination of functional moieties or molecules, as well as accelerating the charge transfer between electrode and analyses/electrolyte.[25] For example, a glucose sensor based on N-doped graphene modified glucose oxidase electrode has reported,[26] which exhibited a higher glucose response than undoped graphene.

In this study, we hybridized a high-surface-area N-doped reduced graphene oxide with ZnO nanoparticles through low temperature, low-cost and one step hydrothermal method. The ZnONFs acted as not only spacers for N-rGO sheets, but also as electro-catalysts for L-cysteine oxidation, which leads to an increase of the surface area and the L-cysteine sensitivity relative to pure ZnO and N-rGO.

2. Experimental

2.1. Reagents and instruments

Graphite (average particle size 30 μm) was purchased from Shanghai Carbon Co., Ltd., China. Graphene oxide (GO) was prepared by using modified Hummers method.[27] All the other reagents were of analytical grade and used as received.

The chemical and physical characterizations of the nanocomposite were investigated by using transmission electron microscopy (TEM, Hitachi S-4800, Japan), field emission-scanning electron microscopy (FE-SEM, JEOL JSM-6700, Japan), X-ray photoelectron spectroscope (XPS, Thermo Fisher Scientific ESCALAB 250Xi, USA) with an Al K_α X-ray source (1486.6 eV) and X-ray diffraction system (XRD, Bruker D8 ADVANCE diffractometer, Germany) with a high power X-ray diffractometer with Cu K_α radiation (35 kV, 20 mA, $\lambda = 1.5$ Å) at a scan rate of 2° (2θ) per min.

2.2. Preparation of the nanocomposite

ZnO nanoparticle-doped N-rGO was prepared in a typical process. Briefly, amount of $ZnSO_4$ was injected into 5 mL of a 1 mg mL^{-1} GO suspension followed by supersonic vibration for about 50 minutes. Subsequently, appropriate amount of $NH_3 \cdot H_2O$ (wt 25%) was added dropwise. The as-prepared suspension was transferred into a high pressure reactor and suffered to hydrothermal reactions at 180 °C for 12 hours. And then, the obtained dark precipitates were washed by centrifugation. Finally, the purified precipitates were dried at 60 °C, and the nanocomposite was obtained for further tests and preparation of sensor.

2.3. Preparation of the nanocomposite modified electrode

Composite carbon paste was prepared by a traditional technique. In short, the above collected nanocomposite was hand ground with appropriate amount of graphite and suitable silicone oil in a mortar for about 1 hour to prepare a uniform paste. Some of the obtained carbon paste was filled into one end of a glassy tube ($d = 3$ mm). Subsequently, a copper wire was inserted deep into the opposite end for an electrical contact. Before use, the electrode surface was polished on a weighing paper. For comparison, a bare CPE, ZnO/CPE and N-rGO/CPE were prepared through the similar procedure.

3. Results and discussion

3.1. Characterizations of the nanocomposite

The preparing procedure of the nanocomposite is displayed in Scheme 1. Firstly, in the mixing process, Zn^{2+} was homogeneously dispersed on GO surface assisted by its oxygen-containing functional group. After the injection of $NH_3 \cdot H_2O$, Zn^{2+} was changed to $Zn(OH)_2$. Under the high temperature of 180 °C and high pressure, the solution was subjected to the

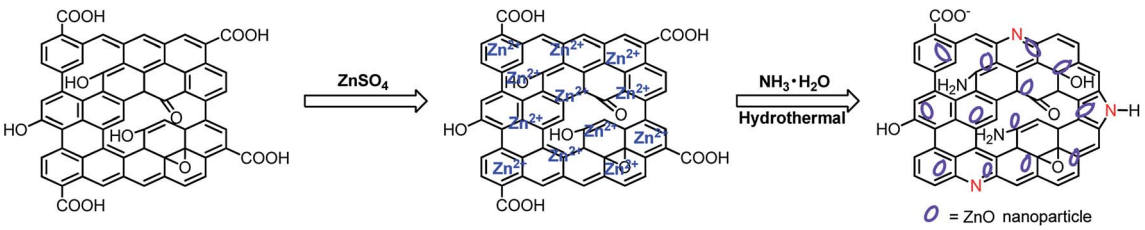

Scheme 1 Illustration of the synthesis of the ZnONPs/N-rGO nanocomposite.

hydrothermal reaction to produce the ZnONPs/N-rGO nanocomposite.

The morphology of the obtained nanocomposite was recorded by SEM and TEM. Fig. 1a clearly displays the SEM image of N-rGO planar sheets with wrinkled and folded features, suggesting that the typical morphology of graphene was also kept after N-doping. As shown in Fig. 1b, the SEM image of ZnONPs/N-rGO nanocomposite shows that numerous ZnONPs disperse equally on the surface of N-rGO. As can be seen from Fig. 1c, transparent flake-like N-rGO is readily observed. It was found that most of the ZnO particles in the range of 80–120 nm, and the average size of around 100 nm was obtained according to the TEM measurement out of 200 nanoparticles. Due to the smooth and planar nanosheets provided by N-rGO sheets, the ZnO can independently form on the nanosheets instead of aggregation.

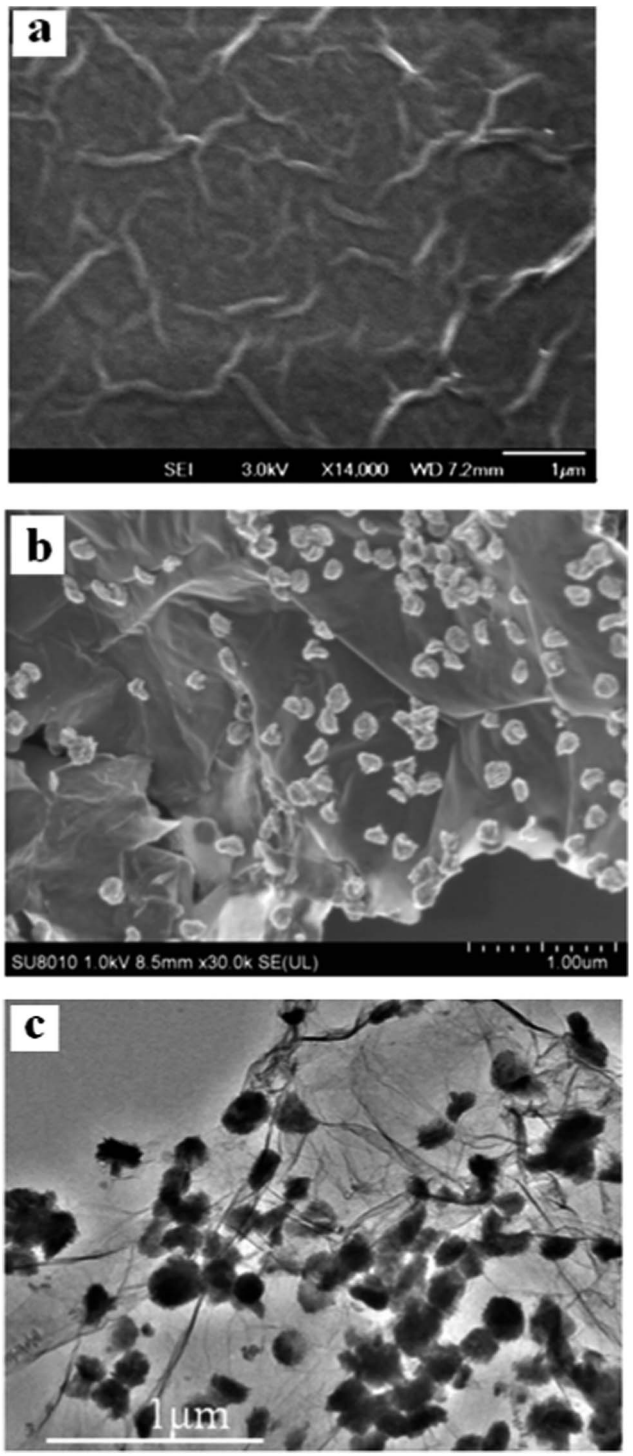

Fig. 1 SEM images of N-rGO (a) and ZnONPs/N-rGO (b), TEM image of ZnONPs/N-rGO (c).

XRD patterns of GO, N-rGO and ZnONPs/N-rGO are shown in Fig. 2. For GO, the characteristic diffraction peak records at 9.9°. After chemically reduction and doping with N, the feature peak of GO at 9.9° disappears. The diffraction peak of N-rGO centered at about 26° is observed due to the hexagonal structure of N-rGO,[28] suggesting the efficient reduction of GO. In the case of ZnONPs/N-rGO, several diffraction peaks are observed in the range of 8–68°. A typical pattern of zincite phase for ZnO (PDF no. 36-1451) could be identified, and a broad peak at about 26° clearly appears, indicating the presence of rGO nanosheets in the nanocomposite.

In order to verify the composition of ZnONPs/N-rGO, XPS measurements were recorded. As shown in Fig. 3a, the XPS survey spectrum suggests that the nanocomposite includes C, O, N and Zn elements, which proves the N doping into the rGO sheets. In the high-resolution C 1s XPS spectrum (Fig. 3b), the deconvoluted four peaks at 284.5, 285.4, 287.0, and 290.2 eV, represent C–C, N–C, C═O, and C–C═O type bonds, respectively.[28,29] In the high-resolution spectrum of N 1s (Fig. 3c), the broad peak could be fitted into four peaks at 398.5, 399.5, 401.3 and 404.0 eV, which are ascribed to the pyridine N, pyrrolic or amine moieties N, graphitic N and weak oxidized N.[30] The pyridinic N in ZnONPs/N-rGO could provide a pair of electrons for the π-conjugated rings, leading to the properties of electron donor for graphene-based materials; the pyrrolic N has rapid charge mobility in N-rGO due to its excellent electron donor properties.[28,31] Notably, the amount of N incorporated in the nanocomposite was found to be 5.49% with a relatively high doping content. The high-resolution scan of Zn 2p in Fig. 3d shows that two peaks appeared at 1022.5 eV and 1045.6 eV could be corresponding to Zn 2p3/2 and Zn 2p1/2, respectively, suggesting the existence of ZnO in the nanocomposite.[21]

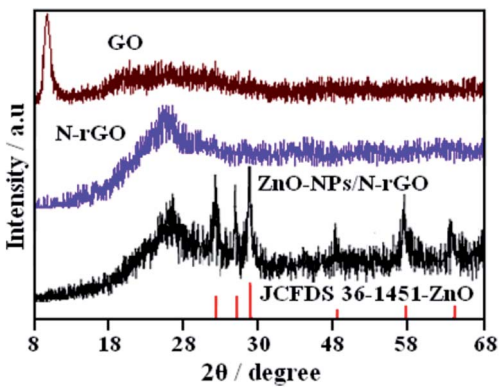

Fig. 2 XRD pattern of GO, N-rGO and ZnONPs/N-rGO.

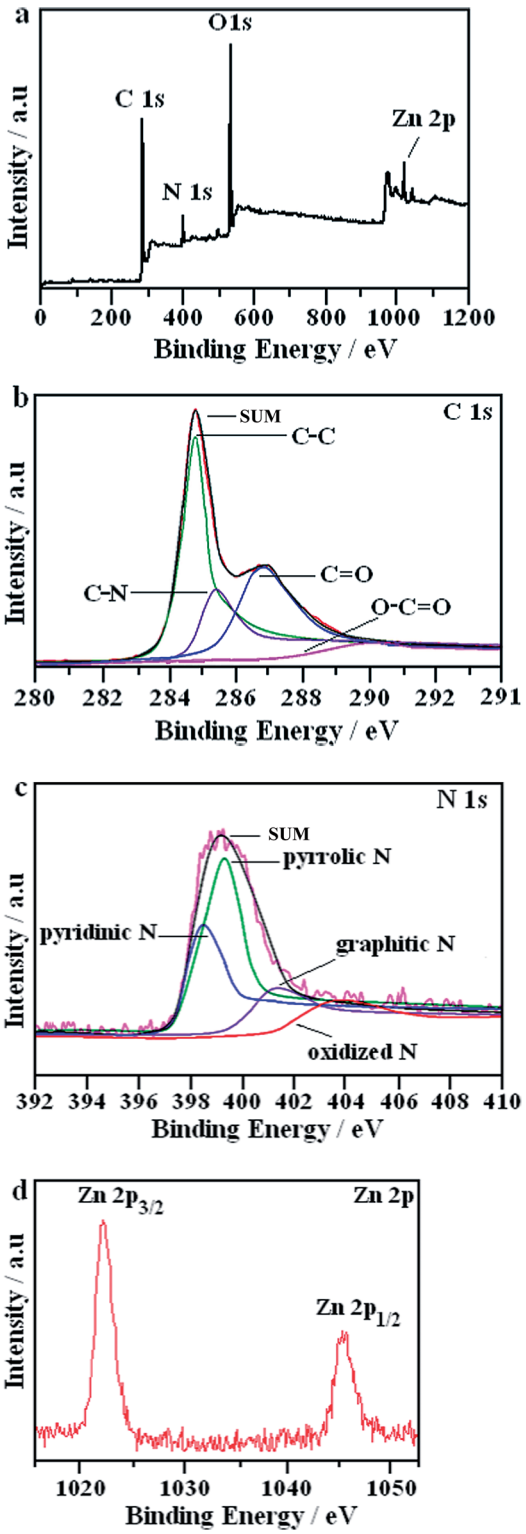

Fig. 3 (a) XPS spectra of ZnONPs/N-rGO and its C 1s (b), N 1s (c) and Zn 2p (d) spectra.

An investigation into the Brunauer–Emmett–Teller (BET) surface areas of the as-prepared samples were performed. Fig. 4 shows the nitrogen adsorption–desorption isotherms of pure ZnO, N-rGO and ZnONPs/N-rGO composite. Bare ZnO and N-rGO have surface areas of 6.09 and 185.40 $m^2\ g^{-1}$ respectively.

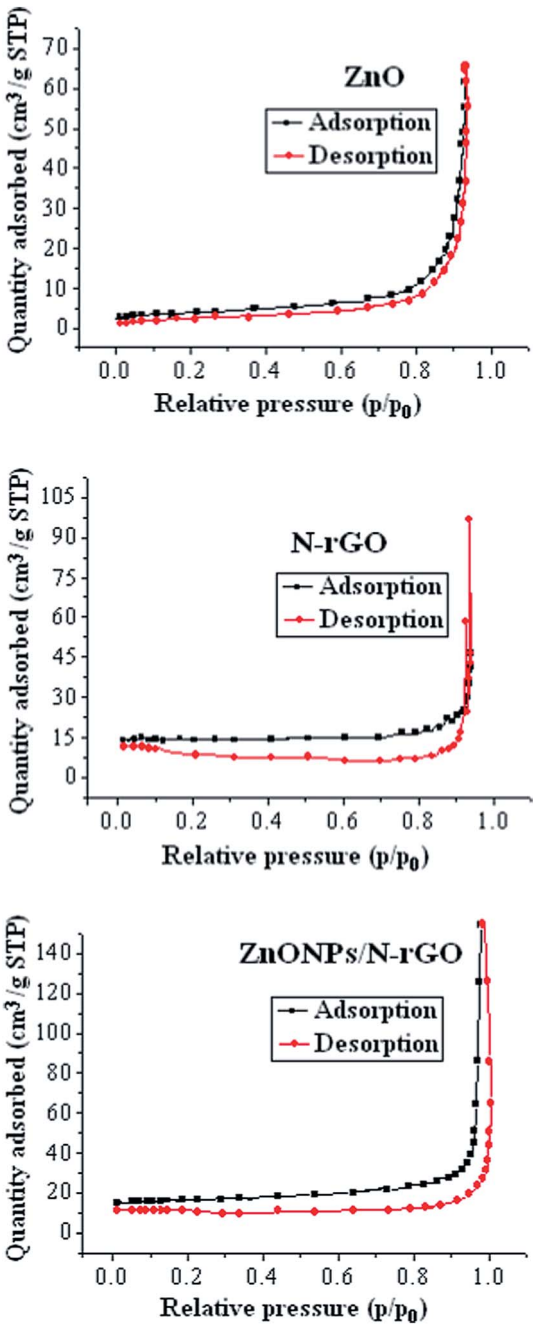

Fig. 4 Nitrogen adsorption and desorption isotherms of pure ZnO, N-rGO and ZnONPs/N-rGO.

ZnONPs/N-rGO has surface areas of 200.55 $m^2\ g^{-1}$. It is clear, therefore, the effect of ZnO particles as an impediment for stacking N-rGO in the composites. This is an evidence to suggest that the incorporation of graphene to ZnO can improve the surface area.

The weight percentage of the ZnO in the ZnONPs/N-rGO composite was obtained by thermogravimetric analysis (TGA), which was conducted from 25 to 800 °C with a heating rate of 10 °C min^{-1} in air. Fig. 5 presents the weight loss of the ZnONPs/N-rGO along with that of the N-rGO. It is worth noting that ZnO remain stable during the heating process, while the N-

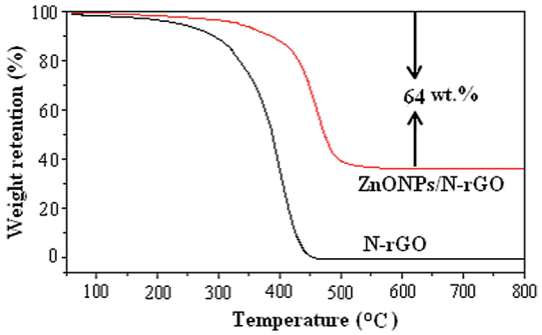

Fig. 5 TGA curves of the N-rGO and the ZnONPs/N-rGO.

rGO in the composite would be completely burned out. Therefore, the 64% weight loss of the composite is entirely from the oxidation of the N-rGO, from which the weight percentage of the ZnO in the composite can be calculated to be 36%.

3.2. Electrochemical characteristics of the modified electrode

Electrochemical impedance spectrum (EIS) is a strong evidence for studying the interface feature of the modified electrodes, which includes a semicircular portion and a linear portion. The semicircle diameter is corresponding to the electron-transfer resistance (R_{et}), indicating the electron transfer kinetics of the redox probe. Fig. 6 displays the impedance spectra of different electrodes, respectively. The bare CPE shows an obvious semicircle (curve c), implying the characteristic of an electron-transfer limited process. After modified ZnO in the electrode, an obvious increasing semicircle interfacial R_{et} is obtained (curve d) since semi-conductive ZnO could act as a barrier to prevent the interfacial charge transfer. The R_{et} of the N-rGO/CPE (curve b) is much smaller than those of CPE and ZnO/CPE, suggesting that N-rGO could serve as a good electron-transfer interface for the electrode and $Fe(CN)_6^{3-/4-}$ to contact. Especially, when the ZnONPs/N-rGO nanocomposite was introduced into CPE, we observe that the diameter decreases further (curve a), indicating that the ZnONPs/N-rGO could more effectively accelerate the electron-transfer, which is ascribed to the synergistic effect of ZnONPs and N-rGO.

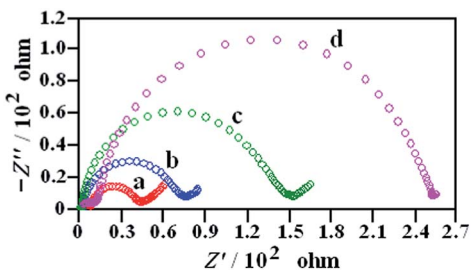

Fig. 6 The EIS of the ZnONPs/N-rGO/CPE (a), N-rGO/CPE (b), CPE (c) and ZnO/CPE (d) in 5.0 mM $Fe(CN)_6^{3-/4-}$ and 0.1 M KCl solution in the frequency range swept 10^5 to 0.1 Hz.

3.3. Electrochemical response of the modified electrode to L-cysteine

Fig. 7A displays the cyclic voltammograms (CVs) of ZnONPs/N-rGO/CPE (a), N-rGO/CPE (b), rGO/CPE (c), ZnO/CPE (d) and CPE (e) in 0.1 M phosphate buffer (pH 9.0) with and without the addition of 10.0 mM L-cysteine. It is readily observed in Fig. 7A that the bare CPE and ZnO/CPE dose not show any redox peak in the potential range with L-cysteine. ZnONPs/N-rGO/CPE dose not display any redox peak in 0.1 M phosphate buffer (pH 9.0) without L-cysteine (f). In contrast, in the presence of 10.0 mM L-cysteine, the ZnONPs/N-rGO/CPE (a), N-rGO/CPE (b) and rGO/CPE (c) provide a clear oxidation peak at 0.60 V, 0.75 V, 0.83 V, respectively. Furthermore, the oxidation peak current on N-rGO/CPE is higher than that of rGO/CPE, suggesting a stronger electrochemical activity and electron conductivity of N-rGO/CPE than rGO/CPE. In addition, the oxidation peak current on ZnONPs/N-rGO/CPE is remarkably higher than that on the N-rGO/CPE and rGO/CPE, indicating a much more electrochemical activity on the direct oxidation of L-cysteine.

The reasons for the excellent electro-catalytic performance toward L-cysteine at ZnONPs/N-rGO/CPE may be deduced as the following: the numerous catalytic active sites and efficient electrical network for the L-cysteine oxidation are afforded by the high-loading and well-distributed ZnONPs directly on N-rGO surface; according to the reported research,[31] the

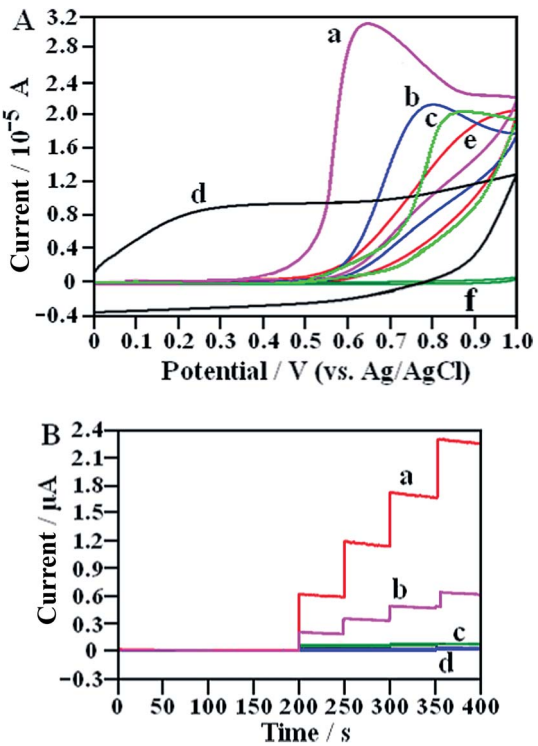

Fig. 7 (A) CVs of ZnONPs/N-rGO/CPE (a), N-rGO/CPE (b), rGO/CPE (c), ZnO/CPE (d) and CPE (e) in the presence of 10.0 mM L-cysteine and ZnONPs/N-rGO/CPE (f) without L-cysteine in 0.1 M phosphate buffer (pH 9.0); scan rate: 100 mV s^{-1}. (B) *i*–*t* curves of ZnONPs/N-rGO/CPE (a), N-rGO/CPE (b), ZnO/CPE (c), and CPE (d) for successive additions of 0.2 mM L-cysteine in 0.1 M phosphate buffer (pH 9.0) at an applied potential of 0.55 V.

pyridinic N at N-rGO can give a pair of electrons for conjugation with the π-conjugated rings, introducing electron donor to N-rGO and improving the electrochemical behaviors of N-rGO. Furthermore, the pyrrolic N has higher charge mobility in N-rGO because of the considerable electron-donor properties and strengthens the carbon catalytic activity in electron transfer reactions. Thus, the electro-catalytic activity of ZnONPs/N-rGO is trusted to be better than pure ZnO. Without a doubt, the synergistic effect of ZnONPs and N-rGO makes the excellent electro-catalytic activity toward the oxidation of L-cysteine.

The current–time (*i*–*t*) curves were recorded to prove the amperometric sensing characteristics of different sensors. As can be seen from Fig. 7B, the current response of ZnONPs/N-rGO/CPE is intensively higher than those of ZnO/CPE, N-rGO/CPE and CPE, indicating the excellent electro-catalytic activity of the nanocomposite toward the oxidation of L-cysteine.

3.4. Amperometric sensing of L-cysteine

The steady-state amperometric response of the modified electrode (ZnONPs/N-rGO/CPE) to L-cysteine was investigated by successive addition of amount of L-cysteine into 10 mL 0.1 M phosphate buffer (pH 9.0) under the optimal conditions. The modified electrode exhibited a fast response to the change concentration of L-cysteine. After the addition of L-cysteine, response current immediately enhanced and reached 98% of steady-state current with in 5 s. Fig. 8 records a typical *i*–*t* graphics for successive addition of L-cysteine with marked concentrations. When the concentration of L-cysteine changes from 0.1 μM to 1.0 mM, the current response corresponding to the concentration have a linear relationship in the ranges of 0.1–205.0 μM and 205.0–705.0 μM, respectively. The regression equations are: $i/\mu A = 0.2945 + 0.0334C/\mu M$ ($r = 0.9979$) for the range of 0.1–205.0 μM and $i/\mu A = 3.7825 + 0.0161C/\mu M$ ($r = 0.9972$) for the range of 205.0–705.0 μM. The different accumulation efficiency at different concentration results in the different slopes of the two calibration curve. The limit of detection was calculated to be 0.1 μM (S/N = 3). The detection performances of the nanocomposite modified electrode compared with sensors based on other modified materials are listed in Table 1. It can be seen that ZnONPs/N-rGO modified electrode has a lower limit of detection or a wider linear range. ZnONPs/N-rGO modified electrode has a wider linear range than AuNPs/PEBT modified electrode. Although, the limit of detection and linear range on ZnONPs/N-rGO modified electrode is lower than AuNPs (0.5%)-nano-ZSM-5 modified electrode, but the prepared procedure of AuNPs (0.5%)-nano-ZSM-5 is complicated, which need a large number of organic reagents (such as TEOS, TPAOH, PrTES, 3-aminopropyl trimethoxysilane, toluene and acetone), as well as high temperature processes, such as hydrothermal treatment at 443 K for 3 days and calcination at 823 K for 4 h under flowing air.

The repeatability of L-cysteine detection was carried out through measuring the current by amperometry in the presence of 0.2 mM L-cysteine. The relative standard deviation (RSD) for 4 times was only 4.1%. Additionally, the stability of sensor was tested. When ZnONPs/N-rGO/CPE was not in use, it was stored

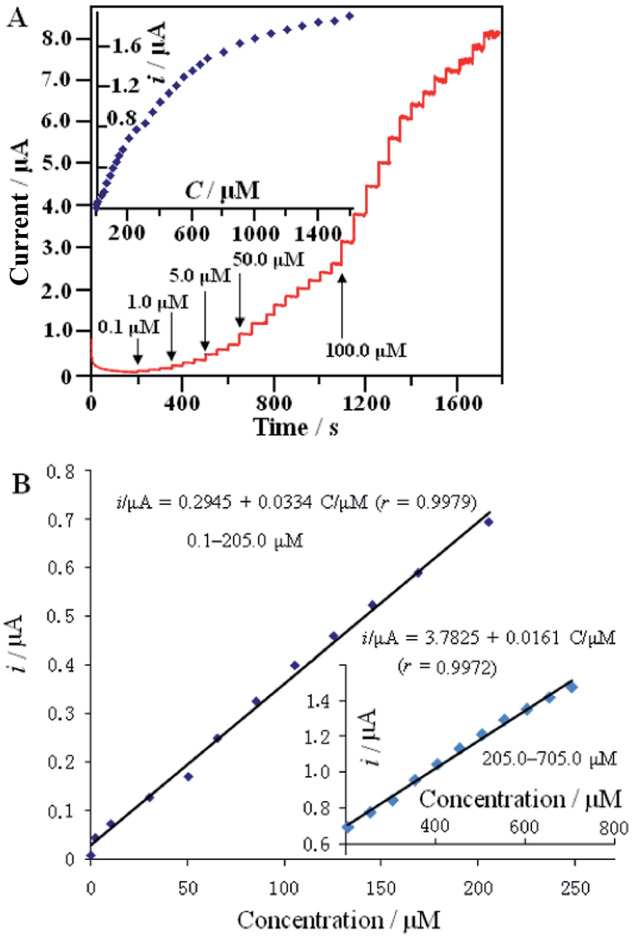

Fig. 8 (A) *i*–*t* response of the modified electrode recorded at 0.55 V with the successive addition of amount of L-cysteine; the inset is plots corresponding to *i* *vs.* *C* of L-cysteine; (B) the linear relationship between the current and concentration of L-cysteine in the range of 0.1–205.0 μM; the inset is the linear relationship between the current and concentration of L-cysteine in the higher range of 205.0–705.0 μM.

at room temperature, 90.0% of the initial current of L-cysteine were remained after 7 days when using once per day, suggesting that the sensor had a good stability.

3.5. Interference study

To investigate the anti-interference capability of the ZnONPs/N-rGO/CPE for the detection of L-cysteine, the important interferents, such as glycine, glucose, dopamine and uric acid were tested during amperometric sensing of L-cysteine. As shown in Fig. 9, the current response of the modified electrode to 0.1 mM L-cysteine is not influenced by injections of 0.1 mM glycine, glucose, dopamine and uric acid according to the relative error ≦±15%. Moreover, chloride ion may easily make some metal or metallic oxide-based sensors to poison and lose their activity. However, the experimental result proves that the modified electrode keep the same response to 0.1 mM L-cysteine in the present of 0.1 M NaCl, indicating that the modified electrode is immune to the poisoning of Cl^-.

Table 1 Comparison of detecting performance of the nanocomposite modified electrode with other modified materials

Electrode material	Sensitivity (μA μM^{-1})	Detection limit (μM)	Linear range (μM)	Ref.
PPy/GQDs@PB/GF	0.41	0.15	0.2–50	8
	0.15		50–1000	
GCE/MWCNTs/$[Fe(CN)_5(P4VP)_{10}]$	0.996	—	0.0205–0.151	9
AuNPs/PEBT	0.0975	0.008	0.05–100	10
AuNPs(0.5%)-nano-ZSM-5	1.4/cm^2	0.0003	0.002–800	12
Cu_2O	0.0020346	—	0.002–0.03	13
GNSs/MnO_x	0.027	0.075	Up to 120	14
MWCNTs–PVP/Cu^{2+}	0.007	1.50	5–60	16
ZnONPs/N-rGO	0.0334	0.1	0.1–205.0	This work
	0.0161		205.0–705.0	

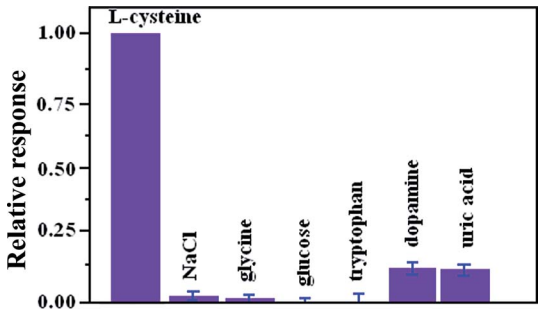

Fig. 9 Influence of addition of some important interferents on the determination of 0.1 mM L-cysteine with ZnONPs/N-rGO/CPE: the interferents are added at the same concentration (10 mL 0.1 mM L-cysteine). The response is normalized with respect to the response of L-cysteine. Error bars represent standard deviation, $n = 3$.

Table 2 Detection and recovery of L-cysteine in dosage forms at a ZnONPs/N-rGO/CPE ($n = 4$)

Sample	Labeled value (mg)	Amount found (mg)	Recovery (%)	RSD (%)
Capsule 1	350	349.6	99.8	4.0
Capsule 2	350	345.4	98.7	3.9
Capsule 3	350	343.3	98.1	4.2

3.6. Application of the modified electrode in real samples

To validate the application of the present sensor in practical analysis, the detection of L-cysteine in the sample dosage forms was tested by analyzing the commercially available L-cysteine capsule samples (Table 2). It was found that the detecting L-cysteine was in good agreement with the labeled values, indicating that the ZnONPs/N-rGO/CPE has a promising potential in practical applications.

4. Conclusions

In summary, ZnO nanoparticles anchoring on N-doped reduced graphene oxide nanocomposite was synthesized successfully through low temperature, low-cost and one step hydrothermal method. This synthetic route can be advantageous for preparing other novel N-doped graphene-based nanocomposites. Moreover, an L-cysteine sensor was fabricated by using the nanocomposite. The fabricated biosensor displayed high electrocatalytic activity toward L-cysteine. This biosensor also provides a promising platform for studying the produce of other metal oxides/N-doped reduced graphene oxide as electrocatalysis in the future. The considerably synergetic effect deriving from the high catalytic nature of ZnO and high electron conductivity of N-rGO also provides the nanocomposite with permission for other bimolecular determination.

Acknowledgements

The authors gratefully acknowledge the financial support from Student Innovation Foundation of Anyang Normal University (No. ASCX/2017-Z32) and Henan Key Laboratory of Biomolecular Recognition and Sensing, Shangqiu Normal University (No. HKLBRSK1601).

References

1 O. Rusin, N. N. S. Luce, R. A. Agbaria, J. O. Escobedo, S. Jiang, I. M. Warner, F. B. Dawan, K. Lian and R. M. Strongin, *J. Am. Chem. Soc.*, 2004, **126**, 438–439.
2 X. Yang, Y. Guo and R. M. Strongin, *Angew. Chem., Int. Ed.*, 2011, **50**, 10690–10693.
3 M. T. Heafield, S. Fearn, G. B. Steventon, R. H. Waring, A. C. Williams and S. G. Sturman, *Neurosci. Lett.*, 1990, **110**, 216–220.
4 Z. Deakova, Z. Durackova, D. W. Armstrong and J. Lehotay, *J. Chromatogr. A*, 2015, **1408**, 118–124.
5 A. Mohammad, A. F. Zahra and H. Tooba, *J. Photochem. Photobiol., A*, 2015, **309**, 8–14.
6 M. Hanieh and Y. Saeed, *Anal. Methods*, 2014, **6**, 8482–8487.
7 W. Liu, J. Luo, Y. M. Guo, J. Kou, B. X. Li and Z. J. Zhang, *Talanta*, 2014, **120**, 336–341.
8 L. Wang, S. Tricard, P. W. Yue, J. H. Zhao, J. Fang and W. G. Shen, *Biosens. Bioelectron.*, 2016, **77**, 1112–1118.
9 C. C. Correa, S. A. V. Jannuzzi, M. Santhiago, R. A. Timm, A. L. B. Formiga and L. T. Kubota, *Electrochim. Acta*, 2013, **113**, 332–339.

10 X. Liu, L. Q. Luo, Y. P. Ding, Z. P. Kang and D. X. Ye, *Bioelectrochemistry*, 2012, **86**, 38–45.
11 M. Murugavelu and B. Karthikeyan, *Superlattices Microstruct.*, 2014, **75**, 916–926.
12 K. Balwinder, S. Rajendra and S. Biswarup, *RSC Adv.*, 2015, **5**, 95028–95037.
13 Z. Dursun and G. Nisli, *Talanta*, 2004, **63**, 873–878.
14 M. S. Mansouri, T. Hazhir and S. Abdollah, *Electroanalysis*, 2013, **25**, 2201–2210.
15 L. G. Shaidarova, S. A. Ziganshina and G. K. Budnikov, *J. Radioanal. Nucl. Chem.*, 2003, **58**, 577–582.
16 C. Silva, C. Carvalho, B. M. Cristina, S. Murilo, C. C. Correa and L. T. Kubota, *Electrochim. Acta*, 2012, **71**, 150–158.
17 L. Sun, R. Shao, L. Tang and Z. Chen, *J. Alloys Compd.*, 2013, **564**, 55–62.
18 A. Wei, L. Xiong, L. Sun, Y. J. Liu and W. W. Li, *Chin. Phys. Lett.*, 2013, **30**, 365–367.
19 C. Xia, N. Wang, L. Wang and L. Guo, *Sens. Actuators, B*, 2010, **147**, 629–634.
20 K. Khun, Z. H. Ibupoto, X. Liu, N. A. Mansor, A. P. F. Turner and V. Beni, *J. Nanosci. Nanotechnol.*, 2014, **14**, 6646–6652.
21 D. Jiang, X. J. Du, Q. Liu, L. Zhou, J. Qian and K. Wang, *ACS Appl. Mater. Interfaces*, 2015, **7**, 3093–3100.
22 L. Panchakarla, K. Subrahmanyam, S. Saha, A. Govindaraj, H. Krishnamurthy, U. Waghmare and C. Rao, *Adv. Mater.*, 2009, **21**, 4726–4730.
23 X. Wang, X. Li, L. Zhang, Y. Yoon, P. K. Weber, H. Wang, J. Guo and H. Dai, *Science*, 2009, **324**, 768–771.
24 H. Liu, Y. Liu and D. Zhu, *J. Mater. Chem.*, 2011, **21**, 3335–3345.
25 X. Wang, G. Sun, P. Routh, D. H. Kim, W. Huang and P. Chen, *Chem. Soc. Rev.*, 2014, **43**, 7067–7098.
26 Y. Wang, Y. Shao, D. W. Matson, J. Li and Y. Lin, *ACS Nano*, 2010, **4**, 1790–1798.
27 S. Gilje, S. Han, M. S. Wang, K. L. Wang and R. B. Kaner, *Nano Lett.*, 2007, **7**, 3394–3397.
28 D. Jiang, Q. Liu, K. Wang, J. Qian, X. Y. Dong, Z. T. Yang, X. J. Du and B. J. Qiu, *Biosens. Bioelectron.*, 2014, **54**, 273–278.
29 C. H. Zhang, L. Fu, N. Liu, M. H. Liu, Y. Y. Wang and Z. F. Liu, *Adv. Mater.*, 2011, **23**, 1020–1024.
30 D. Long, W. Li, L. Ling, J. Miyawaki, I. Mochida and S. H. Yoon, *Langmuir*, 2010, **26**, 16096–16102.
31 S. H. Yang, X. F. Song, P. Zhang and L. Gao, *ACS Appl. Mater. Interfaces*, 2013, **5**, 3317–3322.